5th Annual CDT Conference in Energy Storage & Its Applications, Professor Andrew Cruden, 2021, 01-12, held virtually

The Temperature Stability and Development of a Broadband Silver Nanofluid for Solar Thermal Applications

Harriet Kimpton[ab*], Xunli Zhang[a], Eugen Stulz[b]
[a]*School of Engineering, University of Southampton, University Road, Southampton, SO17 1BJ, UK*
[b]*School of Chemistry, University of Southampton, University Road, Southampton, SO17 1BJ, UK*

Abstract

This paper details an investigation into the synthesis and temperature stability testing of silver-nanofluids, aimed at producing three silver-based nanofluids with distinctive morphologies and absorption characteristics suitable for enhanced efficiency volumetric solar-thermal collectors, which could be combined with a suitable thermal storage system to provide low-carbon heating and hot-water. When combined the three silver-based nanofluids were designed to give spectrally broadband absorption of the incident solar radiation in the 300 – 1300 nm range. The starting point was a previously developed synthesis producing triangular silver-nanoparticles with a strong absorbance in the 850 – 950 nm range (Nanofluid 1). The effect of changing various reagents in the synthesis was then investigated. Increasing the silver nitrate concentration and changing the silver to reducing agent ratio produced Nanofluid 2 (strong absorbance in 650 -750 nm range), containing smaller more rounded triangular nanoparticles. For Nanofluid 3, a two-step synthesis had to be adopted, with a seed nanofluid made initially by lowering the concentration of reducing agent (sodium borohydride) and oxidizing agent (hydrogen peroxide). Additional silver nitrate and reducing agent were added, giving a more concentrated nanofluid, containing small silver nanodiscs, with a 450 nm absorption maximum. These three nanofluids were combined together to give a broadband absorber and for the first time, the stability to a temperature of 70°C measured using UV-vis-IR spectroscopy. Results indicate that although a broadband absorber based on silver can be designed it is not suitable for use without an appropriate stabilization strategy, due to a lack of spectral stability with temperature.

Peer-review under responsibility of the scientific committee of the 5th Annual CDT Conference in Energy Storage and Its Applications, Professor Andrew Cruden, 2021.

Keywords: Solar thermal collectors; thermal storage; silver nanoparticles; nanofluids; stability

1. Introduction

There is an unmet need for low carbon heating and hot water [1]. Widespread heat pump use could decarbonise domestic heating but may destabilise the electricity grid [2]. An alternative approach is to use solar thermal collectors coupled with inter-seasonal storage [3]. To facilitate this it would be useful to improve the efficiencies of current solar thermal collectors. Volumetric absorption utilising engineered colloidal suspensions of nanoparticles or nanofluids have been considered as a means of enhancing solar thermal efficiencies [4]. A volumetric absorber consists of a flowing working fluid, protected by a suitable glazed or glass front face. This working fluid absorbs the solar radiation directly and there is no need for a conventional selective surface absorber. This gives the volumetric absorber certain

* Corresponding author. *E-mail address:* hjk1n15@soton.ac.uk

Peer-review under responsibility of the scientific committee of the 5th Annual CDT Conference in Energy Storage & Its Applications, Professor Andrew Cruden, 2021.

potential advantages, namely simpler manufacturing with less copper [5], a more uniform temperature rise through the fluid system reducing overall heat loss [6], and improved heat transfer [7], leading to an efficiency improvement of ≈ 10% [8]. Improving the properties of the working or nanofluid employed to enhance solar absorbance and other properties such as thermal conductivity and heat capacity could further improve this.

To enhance solar absorbance, the ideal nanofluid needs to absorb solar radiation strongly over the broad range of the solar spectrum with a low concentration of nanoparticles to prevent nanoparticle aggregation in the fluid [9, 10]. Although graphite and metal oxide based nanofluids tend to achieve broadband absorption, they require ≈ 5 x the concentration of metal based nanofluids [11] enhancing possible aggregation. Metal based nanofluids, however, exhibit strong absorption at lower reagent concentrations but tend to have a narrow absorption peak [12]. To overcome these limitations, a blended nanofluid consisting of different gold nanoparticles [9, 12, 13] and with silver nanoparticles [14] have been shown to be suitable for volumetric absorption. The position of the absorption peak (λ_{max}) for silver can be tailored by changing the size and shape of the nanoparticles [15]. It should therefore be possible to combine difference silver nanoparticles with a range of selected sizes and shapes to produce a nanofluid which absorbs over a broad spectral range. This has been shown to be possible numerically [14]. Previously, our work has focused on a synthesis method for producing silver nanoprisms with strong absorption in the 850 – 950 nm range [16-19]. This study uses this as a starting point for the development of other silver nanofluids with distinct geometries and hence absorption maxima positions. The aim was to obtain three different nanofluids with the right absorption spectra and silver reagent concentrations that could then be combined without further processing to give a tailored broadband absorber. Further understanding of the synthesis was required to achieve this. The performance of this broadband absorber and stability with simulated sunlight exposure has been published elsewhere [20] hence this paper focuses on the recipe development of the individual nanofluids and subsequent stability to temperature measurements, therefore complementing and extending this previous publication.

The solar intensity varies asymmetrically with wavelength (λ) as shown in Figure 1A with the highest intensity ≈ 530 nm [21]. The intensity then decreases with increasing λ. Over 85% of the energy is associated with $\lambda < 1300$ nm. Hence, one of the nanofluids needs to have a strong absorption at about 500 nm with a high enough reagent concentration of silver to allow this nanofluid to be combined with the other two nanofluids to produce a peak at 500 nm, but still considerable absorption over as much of the rest of the spectrum as possible. A peak at 500 nm rather than at 530 nm was chosen to still provide sufficient absorption in the 400 -500 nm range, due to the narrow width of the absorption peak for silver. The second nanofluid needs to exhibit an absorption maximum somewhere between 500 nm and 850 nm; an ideal target for this nanofluid would be approximately 650 – 750 nm. The final nanofluid would be the already developed nanofluid with an absorption maximum in the 850 – 950 range.

A number of researchers have investigated the effect of the various reagents used in the thermal synthesis of anisotropic silver nanoparticles [22-24] with somewhat conflicting results, with some researcher arguing that the stabilizing agent tri-sodium citrate is vital to producing silver nanoprisms [22, 24], whereas others state that hydrogen peroxide concentration is the most important shape determining reagent [23]. Increasing the amount of reducing agent $NaBH_4$ in the solution also leads to a red shift in λ_{max} producing nanoprisms [24]. Nanoprisms can also be produced using a seeding process, where small spherical seeds of silver are used to subsequently grow larger anisotropic particles.

Nomenclature

AgNPs	Silver nanoparticles	TSCD	Tri-sodium citrate dehydrate
H_p	Absorption peak height	λ	Wavelength
Hrs	Hours	λ_{max}	Absorption maximum
PVP	Polyvinylpyrrolidone	$\eta_{(300\text{-}1300\ nm)}$	Absorption efficiency over 300-1300 nm
TEM	Transmission electron microscopy		

2. Experimental Methods

All chemicals used are: silver nitrate ($AgNO_3$ 99%), tri-sodium citrate dihydrate (TSCD), Polyvinylpirrolidone (PVP, average molecular weight $AM_w \approx 29{,}000$ gmol^{-1}), hydrogen peroxide (H_2O_2 30 weight %(wt-%)), and sodium

borohydride ($NaBH_4$, 99%), all from Sigma Aldrich and used as purchased. All water employed was Milli-Q (ultra-pure water with a resistivity of ≤ 18.2 MΩcm to prevent accidental contamination of the synthesis and to ensure reproducibility of results).

The starting point was a previously developed synthesis to produce silver nanoparticles (AgNPs) stabilized with PVP and TSCD with λ_{max} in the 850 – 950 nm range [19] (Nanofluid 1). Briefly, 24 mL of aqueous solution at room temperature containing silver nitrate ($AgNO_3$, 0.05 M, 0.05 mL), TSCD (0.10 M, 0.375 mL), PVP (0.70 mM, 0.375 mL) and hydrogen peroxide (H_2O_2, 30 wt.%, 0.125 mL) was stirred vigorously followed by rapid injection of a freshly prepared sodium borohydride solution ($NaBH_4$, 25.00 mM, 1.00 mL) after 7 minutes. After another 30 minutes, the solution colour changed rapidly from yellow to orange, then green to finally blue.

Firstly using nanofluid 1 as a starting point, the effect of overall concentration of reagents was investigated. If silver nanoparticles with a λ_{max} close to 850 nm could be obtained from a solution using higher concentrations of reagents, this gives more flexibility for the 2 other nanofluids to be developed as the overall silver reagent concentration in the mixture needs to be ≈ 3 x the initial concentration used for Nanofluid 1 to give enough broadband absorbance. If increasing the concentration of reagents fails to give the same λ_{max} then this would indicate that the synthesis involved a complex reaction (this is likely given the conflicting literature on the role of the different reagents), increasing the difficulty of developing other nanofluids. The experiments investigating overall reagent concentration are detailed in Table 1 (Denoted A-1 to A-4). The synthesis method already developed (initial reagent concentrations) is A-1 (which also serves as B-1, see below). Secondly, the amount of hydrogen peroxide used was varied as this could be a pivotal reagent [23]. Quantities of other reagents were kept constant. The experiments are shown in Table 1 (B-1 to B-6). Previous work by others [23] has shown that when no hydrogen peroxide is present, the absorption maximum occurs at about 400 nm and silver nanospheres are produced. It was hoped that the position of the absorption peak would vary linearly with hydrogen peroxide concentration as in [23] allowing variation of this reagent to be used to produce the other 2 nanofluids required.

Table 1. Experiments investigating effect of overall reagent concentration, H_2O_2 level and Ag to $NaBH_4$ ratio. Ratio of Ag:TSCD is 1:15 and ratio of Ag:PVP is 1:0.1 in all cases

Sample id	PVP / mM	H_2O_2 / ml	$NaBH_4$ / mM	Ratio of Ag to $NaBH_4$	H_2O_2 relative to initial / %	Sample id	PVP / mM	H_2O_2 / ml	$NaBH_4$ / mM	Ratio of Ag to $NaBH_4$	H_2O_2 relative to initial / %
A-1 / B-1	0.01	0.125	1.0	1:10	100	B-5	0.01	0.025	1.0	1:10	20
A-2	0.02	0.250	2.0	1:10	100	B-6	0.01	0.0	1.0	1:10	0
A-3	0.03	0.375	3.0	1:10	100	C-1	0.03	0.375	1.5	1:5	100
A-4	0.04	0.500	4.0	1:10	100	C-2	0.03	0.375	0.75	1:2.5	100
B-2	0.01	0.100	1.0	1:10	80	C-3	0.03	0.375	1.125	1:3.75	100
B-3	0.01	0.075	1.0	1:10	60	C-4	0.03	0.1875	1.5	1:5	50
B-4	0.01	0.050	1.0	1:10	40	C-5	0.03	0.075	1.5	1:5	20

The effect of changing the Ag to $NaBH_4$, ratio was then investigated. For these experiments, the silver reagent concentration was trebled to 0.3 mM, and the $NaBH_4$ level reduced (Table 1 samples C-1 to C-3). Others have found that increasing the $NaBH_4$ level leads to a red shift in λ_{max}, so a decrease should lead to a blue shift [24]. The effect of reducing the H_2O_2 level at the lower Ag to $NaBH_4$ ratio of 1:5 was also studied (samples C-4 and C-5). It was hoped that this investigation would yield a synthesis recipe for Nanofluid 2 (λ_{max} = 650 - 750 nm) or Nanofluid 3 (λ_{max} ≈ 500 nm) at an appropriate silver reagent concentration to combine with the other nanofluids without further processing.

The penultimate group of experiments investigated the effect of adding more of the reducing agent $NaBH_4$ to the already prepared nanofluids. This aimed to see if it was possible to adjust the position of λ_{max} after the nanofluid was synthesized in a similar manner to how an anisotropic silver nanoprisms is produced using a spherical seed [15]. The experiments are detailed in Table 2. In all cases, the starting or seed nanofluid employed was C-1 from Table 1. As the extra $NaBH_4$ was added as a solution to the already prepared nanofluids, this had the consequence of changing both the final $NaBH_4$ molarity and the other molarities resulting in changes to the final Ag to $NaBH_4$ ratio. Finally, the effect of adding both $AgNO_3$ and more $NaBH_4$ to a seed nanofluid was investigated (Table 2 E-1 and E-2). Again, both the final Ag and $NaBH_4$ molarity increased and changed the final Ag to $NaBH_4$ ratio.

Table 2. Experiments investigating adding more sodium borohydride and silver nitrate to a silver nanoparticle seed solution.

Sample id	Seed nanofluid used	$NaBH_4$ added into 2ml of seed solution (for D-1 to D-7 samples) and into 25ml of seed solution (E-1, E-2) / mM	Ag added to 25 ml seed solution / mM	Final Ag molarity / mM	Final $NaBH_4$ molarity mM	Final Ratio of Ag to $NaBH_4$
D-1	C-1	0.124	0	0.299	1.617	1:5.4
D-2	C-1	0.248	0	0.297	1.733	1:5.8
D-3	C-1	0.369	0	0.296	1.847	1:6.3
D-4	C-1	0.490	0	0.294	1.961	1:6.7
D-5	C-1	0.610	0	0.293	2.073	1:7.1
D-6	C-1	0.728	0	0.291	2.184	1:7.5
D-7	C-1	0.845	0	0.290	2.295	1:7.9
E-1	C-4	0.801	0.160	0.450	2.248	1:5
E-2	C-4	0.412	0.163	0.457	1.882	1:4.1

To produce the broadband mixture, the three most suitable nanofluids recipes for a broadband mixture were selected and the synthesis repeated to check method consistency. The broadband mixture was then designed using the ASTM G173 solar spectrum [21] as reference over a λ range of 300 - 1300 nm as described in [20] to calculate the absorption efficiency ($\eta_{(300\text{-}1300\ nm)}$) for a number of different mixtures and the optimum mixture selected for further testing. Transmission electron microscopy (TEM) analysis of the three optimal nanofluids and the mixture was undertaken to understand the morphology. Further details of the designing of the broadband mixture, the amount of the solar spectrum absorbed at different wavelengths for the 3 nanofluids and the mixture, the TEM including size analysis and subsequent real time measurements of performance of the broadband absorber in a solar simulator are provided in our already published work [20].

To assess the temperature stability of the three nanofluids and the resultant broadband absorber, three 1.5 ml samples of each nanofluid and the broadband mixture were placed in Eppendorfs. The UV-Vis-IR spectra for each samples was then measured and the Eppendorfs placed in an Eppendorf Thermomixer Comfort which was maintained at a temperature of 70°C for the duration of the test. The samples were periodically removed and the UV-Vis-IR spectra measured. Samples were exposed for a total time of 12 hours. The temperature used was similar to the maximum temperature seen in simulated sunlight tests in our previous work on silver nanoprisms [19], but greater than the maximum temperature obtained in the shorter simulated sunlight tests in our broadband work [20].

To characterize the nanoparticles and nanofluids, UV-Vis-IR spectroscopy analysis was employed for the temperature stability assessment using an AvaLight – Hal lamp and Avaspec -2048 with AvaSoft 8.10 software UV-Vis-IR spectrophotometer with an integration number of 1.05 ms and 1000 averages over a λ of 330 to 1100 nm. UV-Vis spectroscopy analysis was also employed using a Varian Cary 300 Bio spectrophotometer over a λ of 200 to 900 nm (scan rate 600 nm min^{-1}, step of 1 nm, time per step 0.1 s). For both a 10 mm path length cuvette was used with samples being diluted appropriately to keep the initial $\lambda_{max} < 2$ au. All initial investigations utilized UV-Vis whereas UV-Vis-IR was used on the temperature assessment of the final optimized nanofluids and resultant broadband mixture.

3. Results and Discussion

Figure 1B shows the effect of changing the overall reagent concentration of the synthesis reagents. At the initial reagent concentration of 0.1 mM Ag, λ_{max} was > 900 nm and the absorption peak height (H_p) was > 1.4 au. As the concentration of reagents increased λ_{max} blue shifted and H_p dropped with the spectra broadening. Samples at higher reagent concentration were diluted to the 0.1 mM Ag equivalent level to allow direct comparison of the spectra and prevent saturation of the UV-Vis detector. A second peak at ≈ 400 nm also started to appear as the reagent concentration increased. H_p for this second peak was almost as high as the primary peak at the highest reagent concentration (sample A-4). Other researchers also observed the presence of two peaks in their UV-Vis spectra when the silver reagent concentration was increased [25], with an alternative seeded synthesis method using polyvinyl alcohol as a stabilizing agent. The inability to produce nanoparticles with a λ_{max} > 800 nm at higher reagent concentrations suggests that controlling the morphology of the resultant nanoparticles to produce the required peak position is likely to be problematic due to a complex relationship between each of the reagents during the synthesis, which is affected not only by the ratio of the various reagents to each other but also by their overall concentrations in

the solution.

When the amount of H_2O_2 was changed, there was a blue shift in the absorbance spectra (see Figure 1C). However, even with sample B-5 the absorption peak was still > 700 nm and H_p had dropped from 1.47 au for B-1 (initial H_2O_2 level) to 0.91 au. The effect of changing H_2O_2 level was therefore non-linear, and it was not possible to produce a nanofluid with a high value of H_p at a $\lambda_{max} \approx 500$ nm using just this method. The sample with no H_2O_2 produced an absorption peak at ≈ 400 nm, which has been attributed to the formation of silver nanospheres [23].

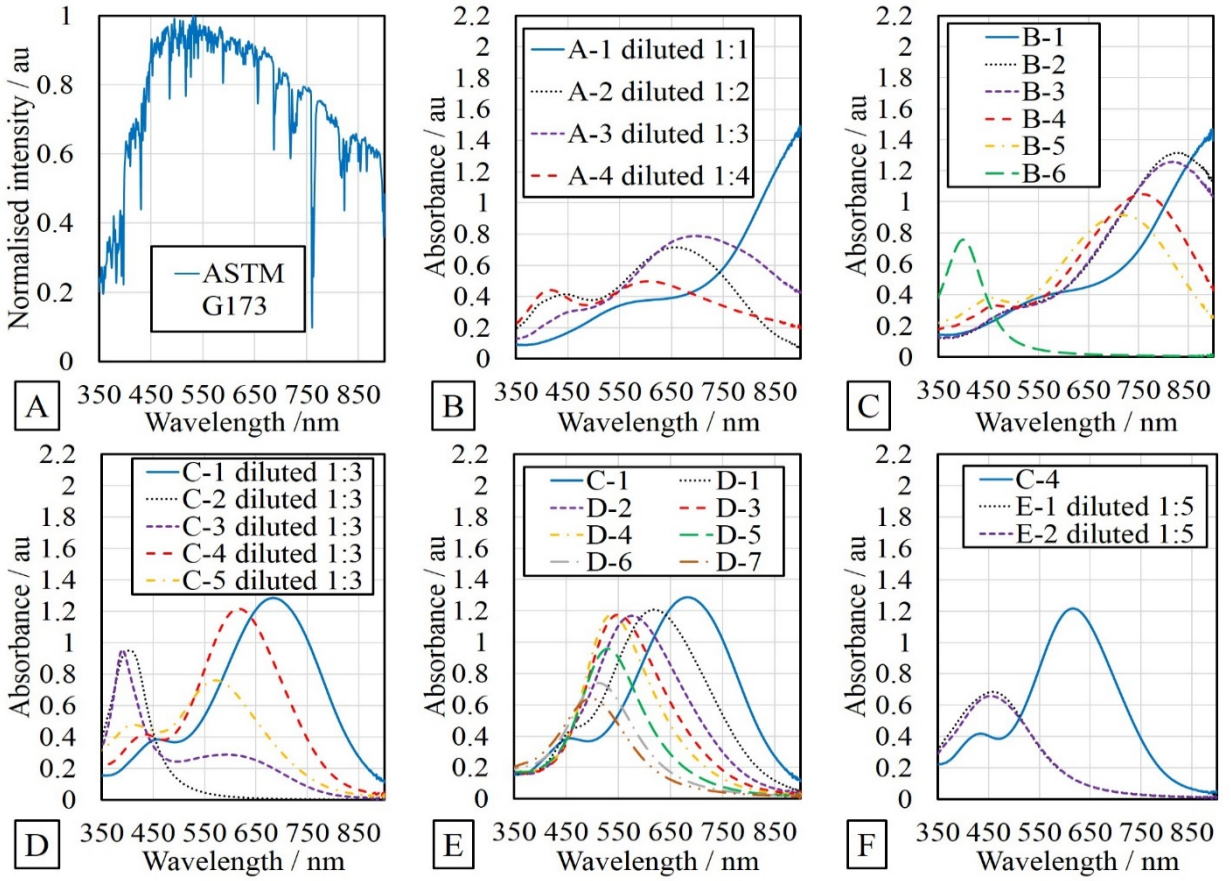

Figure 1 A – ASTM G173 spectrum (adapted from [21]), B-F - UV-Vis spectra showing - B – Effect of reagent concentration, C – Effect of amount of hydrogen peroxide, D – Effect of Ag to $NaBH_4$ ratio, E – Effect of adding $NaBH_4$ to C-1 (all samples in E diluted 1:3) and F – Effect of adding both $AgNO_3$ and $NaBH_4$ to C-4 seed solution (C-4 diluted 1:3). All measurements performed with a 10 mm path length cuvette.

Halving the ratio of Ag to $NaBH_4$ while also increasing the overall concentration of reagents to an Ag reagent concentration of 0.3 mM red shifted λ_{max} to 681 nm (C-1 in Figure 1D). At the same time, H_p only dropped slightly to 1.29 au. This could hence be a suitable recipe for Nanofluid 2 as the mid-λ range absorber. However, further reductions in $NaBH_4$ produced samples with λ_{max} at ≈ 400 nm and not in the 450 - 550 nm range. Again, the relationship between amount of $NaBH_4$ and λ_{max} and H_p was non-linear. This again emphasizes the complex nature of the reaction. When the H_2O_2 amount was halved at the lower Ag to $NaBH_4$ ratio of 1:5 there was a further blue shift in λ_{max} to 616 nm and a slight drop in H_p to 1.22 au (C-4 in Figure 1D). Although the H_p may make this recipe suitable for Nanofluid 2, it is slightly outside the 650 -750 nm ideal range for λ_{max}. Reducing still further the amount of H_2O_2 led to the formation of two peaks (at 571 nm and ≈ 400 nm). There was also a large drop in H_p. It was therefore not possible to identify a suitable recipe for the third short-λ range nanofluid from these experiments.

Figure 1E shows the effect of adding more $NaBH_4$ to a seed nanofluid produced using the recipe for C-1. Surprisingly, the initial effect (D-1) was similar to that obtained when less H_2O_2 was used in the recipe (C-4), with a

shift in λ_{max} to 618 nm and an H_p of 1.21 au. This again emphasizes the complex nature of the synthesis reaction, with $NaBH_4$ normally acting as the reducing agent, whereas H_2O_2 acts as an oxidizing agent to selectively etch the surface of the developing nanoparticle. As more $NaBH_4$ was added, λ_{max} was further red shifted. The level of red shift was reduced as more $NaBH_4$ was added and H_p started to reduce, leading to an almost halving in H_p for D-7, having a λ_{max} of 498 nm. This sample had reached the target value of ≈ 500 nm for Nanofluid 3 (short-λ range) but the reduction in H_p made this a non-ideal synthesis recipe for the production of Nanofluid 3 with a high level of absorbance at 500 nm.

When more Ag^+ and $NaBH_4$ was added to sample C-4 the effect was a red shift of λ_{max} to 457 and 455 nm, (Figure 1F), whilst H_p also dropped to 0.68 and 0.65 au, respectively. However, it should be noted that this value of H_p was for samples diluted 1:5 whereas the molarity of Ag in the actual samples was actually 0.450 and 0.457, respectively (Table 2). If the samples had been diluted to give an Ag molarity of 0.1 mM the corresponding H_p values would have been 0.76 and 0.73 au. This still represents a drop in H_p. The amount of $NaBH_4$ added did not appear to greatly affect the λ_{max} or H_p (compare E-1 and E-2). Either E-1 or E-2 would still be a suitable recipe for the short-λ nanofluid even with the drop in H_p as the overall reagent concentration of Ag was higher allowing for more flexibility in the mixture recipe. E-2 was selected as this had the highest Ag molarity.

The three nanofluids selected for the broadband mixture were A-1 (λ_{max} of 850 - 950 nm), C-1 (λ_{max} 650 – 750 nm) and E-2 (λ_{max} ≈ 460 nm). The ASTM G173 solar spectrum [21] was used to design a mixture with a λ_{max} at around 460 - 500 nm but with as high an absorption as possible in the 850 – 950 nm range as described in [20], giving a final recipe of 30% E-2, 20% C-1 and 50% A-1.

TEM images of the three nanofluids and the resulting mixture were undertaken in our previous publication [20] and show Nanofluid A-1 to consist mainly of triangular particles of ≈ 50 nm size and a thickness of 6 nm, although there were some other smaller disc like particles present. C-1 consisted of smaller (≈ 25 nm) more rounded triangular nanoparticles (thickness ≈ 5 nm), whereas E-2 contained even smaller disc like particles (diameter ≈ 15 nm, thickness 5 nm) and numerous smaller particles ≤ 10 nm in diameter. The mixture contained all the different types of particles. Further discussion of the relationship between morphology and λ_{max} is provided in our previous publication.

The results of the stability to a temperature of 70°C trials are shown in Figure 2. For clarity only the 0, 1 hour and 12 hour data is shown in Figure 2 A-D along with the average values obtained for the three samples. For Nanofluid A-1 initially at time = 0 hours λ_{max} was 873 ± 6.7 nm with an H_p of 1.49 au. This initial value of λ_{max} was less than that seen in Figure 1B for A-1 but between the values of 851 ± 13.6 nm and 926 ± 31.8 nm obtained for the same synthesis in our previously published work [19, 20]. The differences in λ_{max} seen for the nominally identical synthesis show the difficulties in controlling the synthesis using the batch process to produce sharp cornered triangular nanoparticles. The sharpness of the corners is hard to control and others have shown numerically that even a small change in the roundness of the corners can lead to a shift in λ_{max} of up to 200 nm [26]. The value of H_p was slightly lower at 1.49 au than seen previously (1.57 and 1.56 au). After 1 hour at 70°C, λ_{max} had blue shifted to a value of 830 ± 20.6 nm, a change of approximately 40 - 50 nm. The rate of change then slowed considerably with λ_{max} still being 816 ± 18.2 nm after 12 hours. Others have also observed a blue shift in λ_{max} on heating [27]. One of the samples was more stable than the other 2 (see Figure 2E). This difference in stability between samples was also observed for this nanofluid in simulated sunlight exposure tests [19], however, the blue shift was less than the 100 nm shift observed in simulated sunlight. Simulated sunlight both exposes the sample to light and a temperature rise so is a more harsh testing environment. This paper allows for the separation of the temperature effect from the effect of light showing that temperature alone leads to about half the blue shift for Nanofluid A-1 than light / temperature combined. The rate of change of λ_{max} is similar under both conditions with the bulk of the change in λ_{max} occurring in the first hour of exposure.

For Nanofluid C-1 initially at time = 0 hours λ_{max} was 637 nm with an H_p of 1.25 au (Figure 2B). This initial value of λ_{max} was less than that seen for C-1 in Figure 1D and for the repeat synthesis in our previous publication of 667 ± 7.9 nm [20], however, H_p was similar. On exposure to a temperature of 70°C, there was a blue shift in λ_{max} of about 90 nm with a small increase in H_p to 1.33 au after 1 hour. This change in λ_{max} was similar to that seen after 30 minutes in simulated sunlight, however, the change in H_p although in the same direction was not as great for temperature alone. In a similar manner to A-1, the bulk of the change in the spectra for C-1 occurred in the first hour of temperature exposure (Figure 2E) and there was a similar variation in stability between the samples tested. Nanofluid C-1 was therefore more unstable to temperature alone than Nanofluid A-1.

In the temperature tests, initially Nanofluid E-2 had a λ_{max} of 493 nm with an H_p of 1.04 au (Figure 2C). Both these

values were greater than those seen for E-2 in Figure 1F and for the same nanofluid in our previous publication [20]. These differences for Nanofluid C-1 and E-2 illustrate that further work is needed on understanding and improving the variation in the synthesis of these nanofluids. On exposure to temperature for E-2, λ_{max} did not change, but H_p increased to 1.35 au after 1 hour at 70°C. In comparison under simulated sunlight, this nanofluid exhibited a small red shift in λ_{max} and an increase in H_p of about 45% after 30 minutes exposure [20], showing that temperature alone is responsible for some but not all of the changes observed under simulated sunlight.

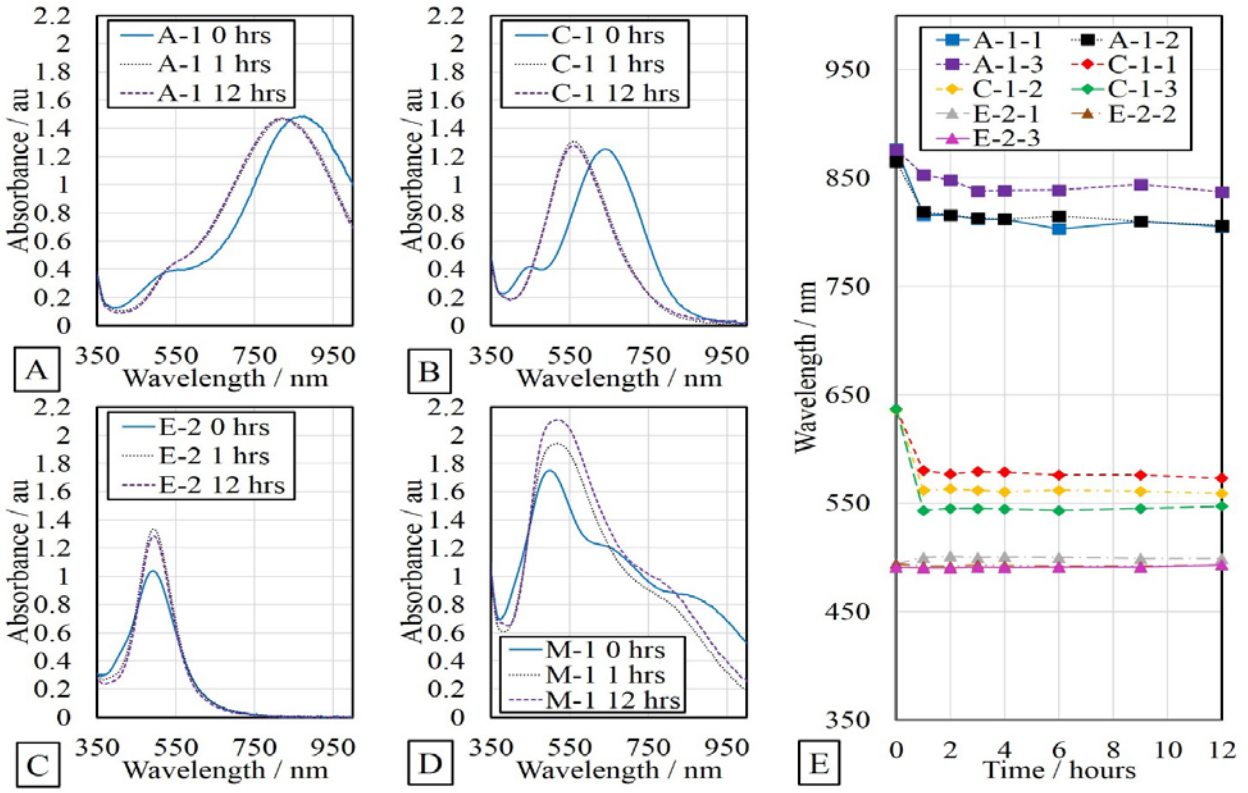

Figure 2 A-D - UV-vis-IR spectra showing change in spectra with exposure to a temperature of 70°C (hours = hrs) for A – Nanofluid A-1, B – Nanofluid C-1 (diluted in the ratio 1:3), C – Nanofluid E-2 (diluted in the ratio 1:5) and D – The broadband mixture (denoted M-1) comprising 30% E-2, 20% C-1 and 50% A-1. Average values from 3 samples shown. All measured with a 10 mm path length cuvette. E- Change in λ_{max} with exposure to a temperature of 70°C (A-1 squares, C-1 diamonds and E-2 triangles, repeat samples denoted as -1, -2 and -3).

The broadband mixture (M-1) consisting of 30% E-2, 20% C-1 and 50% A-1 is shown before and after temperature testing in Figure 2D. Initially the influence of the 3 separate nanofluids on the shape of the spectrum can clearly be seen with a large primary peak corresponding to Nanofluid E-2 being present at 499 nm (H_p = 1.72 au), a pronounced shoulder at about 650 nm corresponding to C-1, and another at about 870 nm corresponding to A-1. However after being exposed to temperature the height of the primary peak increases significantly, the shoulder corresponding to C-1 disappears and the other shoulder is blue shifted to about 780 nm. The change in the spectrum for M-1 is consistent with the red shift observed for A-1 and C-1 and the increase in H_p observed for C-1 and E-2. It is also similar to that observed for the broadband mixture in simulated sunlight testing [20] after 30 minutes exposure.

The change in the morphology of the nanofluids following simulated sunlight exposure which could result in the changes in the spectra observed has been investigated in our previous work [20] and was found to be primarily due to a rounding of the corners of the triangles in A-1 and a further rounding of the rounded triangles to become more disc like in C-1. It is likely that a similar process is occurring with temperature as this rounding of corners corresponding to a blue shift in λ_{max} has also been observed for silver nanoprisms by other researchers [27-29]. TEM analysis of the

nanofluids before and after temperature testing would be needed to confirm this.

It may also be possible to re-design the final broadband absorber, taking into account the potential spectral changes that occur in the first hour of exposure to either temperature or simulated sunlight. Even then it would be challenging to maintain the performance of the absorber in the >800 nm region as the sharp corners of the nanoprisms would be hard to stabilize as they are thermodynamically more unstable [27] and even a small change in the amount of rounding of the corners can lead to a large 200 nm blue shift in λ_{max} [26]. Hence, even with modification of the broadband mixture an appropriate stabilization strategy, such as SiO_2 coating [29] would be needed to make this absorber more suitable for solar or heat applications.

Another option would be to use a mixed broadband absorber containing gold and silver nanoparticles, however, although also tunable, gold is more expensive and the effect of using a mixed system on the stability to temperature and sunlight would have to be carefully assessed. It is already known that even gold nanorods change shape becoming more spherical leading to a blue shift in λ_{max} with exposure to temperature [9], so it is likely that a mixed nanoparticle broadband system based on gold and silver would still be unsuitable for solar applications without a suitable stabilization strategy and considerable further investigation and optimization.

4. Conclusions

By varying the amount and timing of the reagents added during the synthesis of silver nanofluids it allowed for the development of recipes to produce 3 different morphologies of silver nanoparticles, which gave 3 distinct absorption profiles covering a broad range of wavelengths. These were combined to give a broadband absorber tailored to the incident solar radiation. This and our already published work [20] is one of the first studies to deliberately synthesise and measure using UV-Vis-IR a broadband absorber based on silver nanofluids. A potentially better performing broadband absorber based on 5 different types of silver nanoparticles has been designed by others using a numerical study but that broadband absorber was not synthesised experimentally [14]. This is also the first study to investigate the effect of temperature alone on the stability of the developed broadband mixture and its components and as such complements our already published works on simulated sunlight stability [19, 20]. With exposure to temperature the spectra of the individual nanofluids changed rapidly within the first hour of testing and then remained largely stable. This and our previous publications, show that without further stabilization of the nanoparticle shapes to prevent morphological changes with exposure to temperature and sunlight, the developed broadband absorber would not be suitable for solar applications.

This work has also highlighted the difficulties associated with investigating and controlling the nanofluid synthesis, due to the complex reaction that occurs to produce the different shapes of nanoparticles. Further development of optimal synthesis methods is on-going in our laboratories.

Declaration of Competing Interest

We have no conflicts of interest to disclose, however, we would like to acknowledge the University of Southampton for providing funding.

Acknowledgements

The authors would like to acknowledge the support of the Faculty of Engineering and Physical Sciences at the University of Southampton, and the Engineering and Physical Sciences Research Council (EPSRC) through the Centre for Doctoral Training in Energy Storage and its Applications (EP/L016818/1) at the University of Southampton.

Appendix A. Supplementary material

The data supporting this study is available from the University of Southampton repository at http://dx.doi.org/10.5258/SOTON/xxxx to be advised at proof stage.

References

[1] Committee on Climate Change. 2019. Net Zero Technical Report, 7 Holbein Place, London, SW1W 8NR Available: www.theccc.org.uk/publications (Accessed: 07 May 2019).

[2] R. Sansom. 2012. The Impact of Future Heat Demand Pathways on the Economics of Low Carbon Heating Systems, presented at the BIEE-9th Academic Conference, Oxford, UK, 2012.

[3] H. Kimpton, X. Zhang and E. Stulz. 2020. Decarbonising heating and hot water using solar thermal collectors coupled with thermal storage: The scale of the challenge, Energy Reports, 6, 25-34, https://doi.org/10.1016/j.egyr.2020.02.024.

[4] N. Goel, R.A. Taylor and T. Otanicar. 2020. A review of nanofluid-based direct absorption solar collectors: Design considerations and experiments with hybrid PV/Thermal and direct steam generation collectors, Renewable Energy, 145, 903-913, https://doi.org/10.1016/j.renene.2019.06.097.

[5] H. Tyagi, P. Phelan and R. Prasher. 2009. Predicted Efficiency of a Low-Temperature Nanofluid-Based Direct Absorption Solar Collector, Journal of Solar Energy Engineering, 131, 4, 041004, https://doi.org/10.1115/1.3197562.

[6] G. Xu, W. Chen, S. Deng, X. Zhang and S. Zhao. 2015. Performance Evaluation of a Nanofluid-Based Direct Absorption Solar Collector with Parabolic Trough Concentrator, Nanomaterials, 5, 4, 2131-2147, https://doi.org/10.3390/nano5042131.

[7] S.Y. Lee, S.H. Jin, S.M. Kim and J.W. Kim. 2016. Solution plasma process to synthesize silver nanofluids and their thermal conductivity behaviors, Metals and Materials International, 20, 4, 695-699, https://doi.org/10.1007/s12540-014-4014-1.

[8] M. Turkyilmazoglu. 2016. Performance of direct absorption solar collector with nanofluid mixture, Energy Conversion and Management, 114, 1-10, https://doi.org/10.1016/j.enconman.2016.02.003.

[9] J. Jeon, S. Park and B.J. Lee. 2014. Optical property of blended plasmonic nanofluid based on gold nanorods, Opt Express, 22 Suppl 4, A1101-11, https://doi.org/10.1364/OE.22.0A1101.

[10] O.Z. Sharaf, N. Rizk, C.P. Joshi, M. Abi Jaoudé, A.N. Al-Khateeb, D.C. Kyritsis, *et al.* 2019. Ultrastable plasmonic nanofluids in optimized direct absorption solar collectors, Energy Conversion and Management, 199, https://doi.org/10.1016/j.enconman.2019.112010.

[11] N.E. Hjerrild, S. Mesgari, F. Crisostomo, J.A. Scott, R. Amal and R.A. Taylor. 2016. Hybrid PV/T enhancement using selectively absorbing Ag–SiO_2/carbon nanofluids, Solar Energy Materials and Solar Cells, 147, 281-287, https://doi.org/10.1016/j.solmat.2015.12.010.

[12] M. Du and G.H. Tang. 2016. Plasmonic nanofluids based on gold nanorods/nanoellipsoids/nanosheets for solar energy harvesting, Solar Energy, 137, 393-400, https://doi.org/10.1016/j.solener.2016.08.029.

[13] J. Jeon, S. Park and B.J. Lee. 2016. Analysis on the performance of a flat-plate volumetric solar collector using blended plasmonic nanofluid, Solar Energy, 132, 247-256, https://doi.org/10.1016/j.solener.2016.03.022.

[14] A.R. Mallah, S.N. Kazi, M.N.M. Zubir and A. Badarudin. 2018. Blended morphologies of plasmonic nanofluids for direct absorption applications, Applied Energy, 229, 505-521, https://doi.org/10.1016/j.apenergy.2018.07.113.

[15] J. Haber and K. Sokolov. 2017. Synthesis of Stable Citrate-Capped Silver Nanoprisms, Langmuir, 33, 40, 10525-10530, https://doi.org/10.1021/acs.langmuir.7b01362.

[16] M. Carboni, L. Capretto, D. Carugo, E. Stulz and X. Zhang. 2013. Microfluidics-based continuous flow formation of triangular silver nanoprisms with tuneable surface plasmon resonance, Journal of Materials Chemistry C, 1, 45, 7540, https://doi.org/10.1039/c3tc31335b.

[17] M. Carboni. 2014. Silver Nanoprisms Embedded in a Polymeric Matrix for Energy Saving Glazing, Doctor of Philosophy PhD thesis, Faculty of Engineering and the Environment, Southampton.

[18] T. Mabey, D. Andrea Cristaldi, P. Oyston, K.P. Lymer, E. Stulz, S. Wilks, *et al.* 2019. Bacteria and nanosilver: the quest for optimal production, Crit Rev Biotechnol, 39, 2, 272-287, https://doi.org/10.1080/07388551.2018.1555130.

[19] H. Kimpton, D.A. Cristaldi, E. Stulz and X. Zhang. 2020. Thermal performance and physicochemical stability of silver nanoprism-based nanofluids for direct solar absorption, Solar Energy, 199, 366-376, https://doi.org/10.1016/j.solener.2020.02.039.

[20] H. Kimpton, E. Stulz and X. Zhang. 2020. Silver nanofluids based broadband solar absorber through tuning nanosilver geometries, Solar Energy, 208, 515-526, https://doi.org/10.1016/j.solener.2020.08.018.

[21] ASTM. 2012. Reference Solar Spectral Irradiance: American Standard Testing Methods (ASTM), ASTM G-173, Available: https://rredc.nrel.gov/solar//spectra/am1.5/ASTMG173/ASTMG173.html [Accessed: 01 July 2019].

[22] G.S. Metraux and C.A. Mirkin. 2005. Rapid Thermal Synthesis of SIlver Nanoprisms with Chemically Tailorable Thickness, Advanced Materials, 17, 4, 412-415, https://doi.org/10.1002/adma.200401086.

[23] Q. Zhang, N. Li, J. Goebl, Z. Lu and Y. Yin. 2011. A systematic study of the synthesis of silver nanoplates: is citrate a "magic" reagent?, J Am Chem Soc, 133, 46, 18931-9, https://doi.org/10.1021/ja2080345.

[24] X. Dong, X. Ji, J. Jing, M. Li, J. Li and W. Yang. 2010. Synthesis of Triangular Silver Nanoprisms by Stepwise Reduction of Sodium Borohydride and Trisodium Citrate, J. Phys. Chem C, 114, 2070-2074, https://doi.org/10.1021/jp909964k.

[25] J. Walshe, G. Amarandei, H. Ahmed, S. McCormack and J. Doran. 2019. Development of poly-vinyl alcohol stabilized silver nanofluids for solar thermal applications, Solar Energy Materials and Solar Cells, 201, https://doi.org/10.1016/j.solmat.2019.110085.

[26] K. Kelly, E. Coronado, L. Zhao and G. Schatz. 2003. The Optical Properties of Metal Nanoparticles: The Influence of SIze, Shape, and Dielectric Environment, Journal of Physical Chemistry B, 107, 668-677, https://doi.org/10.1021/jp026731y.

[27] B. Tang, S. Xu, X. Hou, J. Li, L. Sun, W. Xu, *et al*. 2013. Shape evolution of silver nanoplates through heating and photoinduction, ACS Appl Mater Interfaces, 5, 3, 646-53, https://doi.org/10.1021/am302072u.

[28] J. Roh, H.N. Umh, H.K. Sung, B.-c. Lee and Y. Kim. 2012. Repression of photomediated morphological changes of silver nanoplates, Colloids and Surfaces A: Physicochemical and Engineering Aspects, 415, 449-453, https://doi.org/10.1016/j.colsurfa.2012.09.018.

[29] R.A. Taylor, N. Hjerrild, N. Duhaini, M. Pickford and S. Mesgari. 2018. Stability testing of silver nanodisc suspensions for solar applications, Applied Surface Science, 455, 465-475, https://doi.org/10.1016/j.apsusc.2018.05.201.